Two-dimensional MXenes as catalytic "flying carpets" to transport biomass valorization towards new horizons: the case of furfural catalytic transfer hydrogenation over noble-metal free niobium-based carbides

Sebastiano Campisi,[a] Antonella Gervasini,[a] Laura Prati,[a] Xiaodong Zhang,[b] Kun Liang,[c] Michael Naguib*,[c] and Alberto Villa*,[a]

[a] Dipartimento di Chimica, Università degli Studi di Milano, via C. Golgi 19, 20133 Milano, Italy

[b] Department of Chemistry, Tulane University, New Orleans, LA, 70118, USA

[c] Department of Physics and Engineering Physics, Tulane University, 6823 St Charles Ave, New Orleans LA 70118, USA

**Corresponding authors:*

Prof. Alberto Villa, e-mail: alberto.villa@unimi.it

Prof. Michael Naguib, e-mail: naguib@tulane.edu

Abstract

The reductive conversion of biomass-derived furfural through catalytic transfer hydrogenation (CTH) over non-precious metal catalysts is regarded as a promising strategy to successfully implement the biorefinery concept. Here, we show that two-dimensional niobium carbides (MXenes) efficiently catalyze the liquid-phase CTH of furfural in the presence of 2-propanol as hydrogen donor.

At 160 °C Nb_2CT_x and $Nb_4C_3T_x$ showed remarkable initial activity values (130 and 73 h^{-1}, respectively), exceeding the one of pure Nb_2O_5 (21 h^{-1}) by factor of 6.2 and 3.5. A targeted surface characterization by acid site titrations and X-ray photoelectron spectroscopy allowed to correlate the catalytic behavior with the acidic features and the peculiar surface chemistry of Nb-MXenes species. The presence of strong acid sites in Nb_2CT_x was associated to high initial activity, but also to a pronounced tendency to undergo deactivation. Differently, $Nb_4C_3T_x$, despite the lower initial activity, assured 70% of furfural conversion after 8 h and it showed good stability over six runs. This study could bring new opportunities for the rational design of advanced noble metal-free catalysts with enhanced activity for biomass valorization.

1. Introduction

Climate changes and fossil fuel depletion are sparking a transition towards a greener and sustainable chemistry, already underway, but which needs to be further promoted to deliver actual benefits to the environment and the economy. This allows for stimulus to the development of novel processes, which require active, eco-friendly and cost-effective catalysts to process biomass feedstocks and obtain platform molecules to be converted into several value-added compounds.

Furfural has been widely recognized as a hemicellulose-derived building block to produce a plethora of fuels, solvents, intermediates and fine chemicals.[1]

Specifically, the reductive conversion of furfural can generate interesting chemical compounds, such as furfuryl alcohol (FA, commonly used as monomer for resins), 2-methylfuran (2-MF, fuel additive and intermediate for drugs, pesticides, flavours or fragrances) and tetrahydrofurfuryl alcohol (THFA, key intermediate in pharmaceutical industry).[2] Indeed, the coexistence of two different reducible moieties (the furfural ring and the carbonyl group) in the furfural molecule causes the reaction to proceed through diverse routes as described in Scheme 1. Experimental conditions as well as catalyst properties (metal nature, structural features, metal support interactions) can direct the selectivity in such a complex reaction pathway.[3,4] Among heterogeneous catalysts, noble metal-based catalysts, *viz.* supported Pd, Pt, Rh, Ir, Ru and Au NPs, assure high activity and selectivity.[5–9] However, economic considerations foster the development of alternative and less expensive catalytic systems. In this view, transition metal carbides (TMCs, where TM = W, Ti, V, Zr, Nb, Mo, Ta) represent a promising noble metal-free solution for dehydrogenation and hydrogenation reactions.[10–14] In particular β-molybdenum carbide (β-Mo_2C) and cobalt-modified Mo_2C emerged as promising no precious metal catalysts for the selective vapor-phase hydrodeoxygenation of furfural.[15–17] The preferential adsorption of furfural molecule onto Mo_2C/Mo(110) surface through the C=O group resulted in a strong interaction, responsible for very high selectivity to 2-methylfuran.[18] In the liquid-phase furfural hydrogenation α-MoC demonstrated to be

more active than β-Mo_2C and the selectivity was controlled by the solvent, being furfuryl alcohol preferentially formed in methanol whereas 2-MF predominated in 2-butanol.[19] The addition of nickel produced Ni–Mo carbide catalysts with high activity and enhanced formation of over-hydrogenated products, namely tetrahydrofurfuryl alcohol and 2-methyltetrahydrofuran (2-MTHF). [20] Ni-W_2C carbides are also known to be highly efficient bifunctional catalysts for the hydrogenolysis of hydroxymethylfurfural to dimethylfurfural.[21]

The family of carbide materials has expanded including a new group of two-dimensional (2D) transition metal carbides, nitrides and carbonitrides, so-called MXenes,[22,23] with exceptional electrical, mechanical, and chemical properties that confer unique potential for several applications, including energy storage, electronics, adsorption, environmental remediation, biomedical, catalysis and electrocatalysis.[23–30] MXenes have chemical formula $M_{n+1}X_nT_x$, where M is an early transition metal element, X stands for carbon and/or nitrogen, T_x represents surface terminated functional group (-O, -F, –OH *etc.*), and n =1-4. [22]They can be derived from layered ternary carbide precursors, MAX phases (where A is an element from groups 13 or 14, *e.g.*, Al or Si) by the selective removal of A layer group, the replacement of the primary M-A bonds with terminations and the formation of atomically thin metal carbide/nitride layers. The peculiar 2D morphology of MXenes endow them with increased surface area compared to the bulk carbides,[31] while the presence of numerous surface terminations imparts hydrophilicity and surface reactivity. Consequently, MXenes can be successfully used as heterogeneous catalysts and supports for catalytic and electrocatalytic reactions. [25,28,30–36]

Concerning the specific biomass-valorization field, recently Ti-based MXenes have been demonstrated to efficiently catalyse the catalytic transfer hydrogenation of furfural to furfuryl alcohol.[37] These results encouraged the exploration of other MXenes as catalysts in furfural hydrogenation. In particular, 2D $Nb_4C_3T_x$ MXene has exhibited an excellent catalytic activity in enhancing the hydrogen storage properties of MgH_2 thanks to its unique layered structure and the *in situ* formation of NbH_x adducts.[33]

On the other hand, niobium-containing solid materials have been extensively exploited as water-tolerant acid solid catalysts in several reactions for biomass processing [38,39,48–50,40–47]. Recently, niobium oxide modified by incorporation of dopants (W^{6+} and Ti^{4+}) has been successfully employed as support in Pt-based catalysts for furfural hydrogenation, unveiling the crucial role of support Lewis acidity in diverting the reaction selectivity.[51] Starting from these considerations, in this work multilayered Nb_2CT_x and $Nb_4C_3T_x$ MXenes were evaluated as catalysts for the catalytic transfer hydrogenation (CTH) of furfural using 2-propanol as the hydrogen source. In general, to the best of our knowledge, this is the first study reporting the use of Nb-carbides as catalysts in hydrogenation reactions of organic substrates.

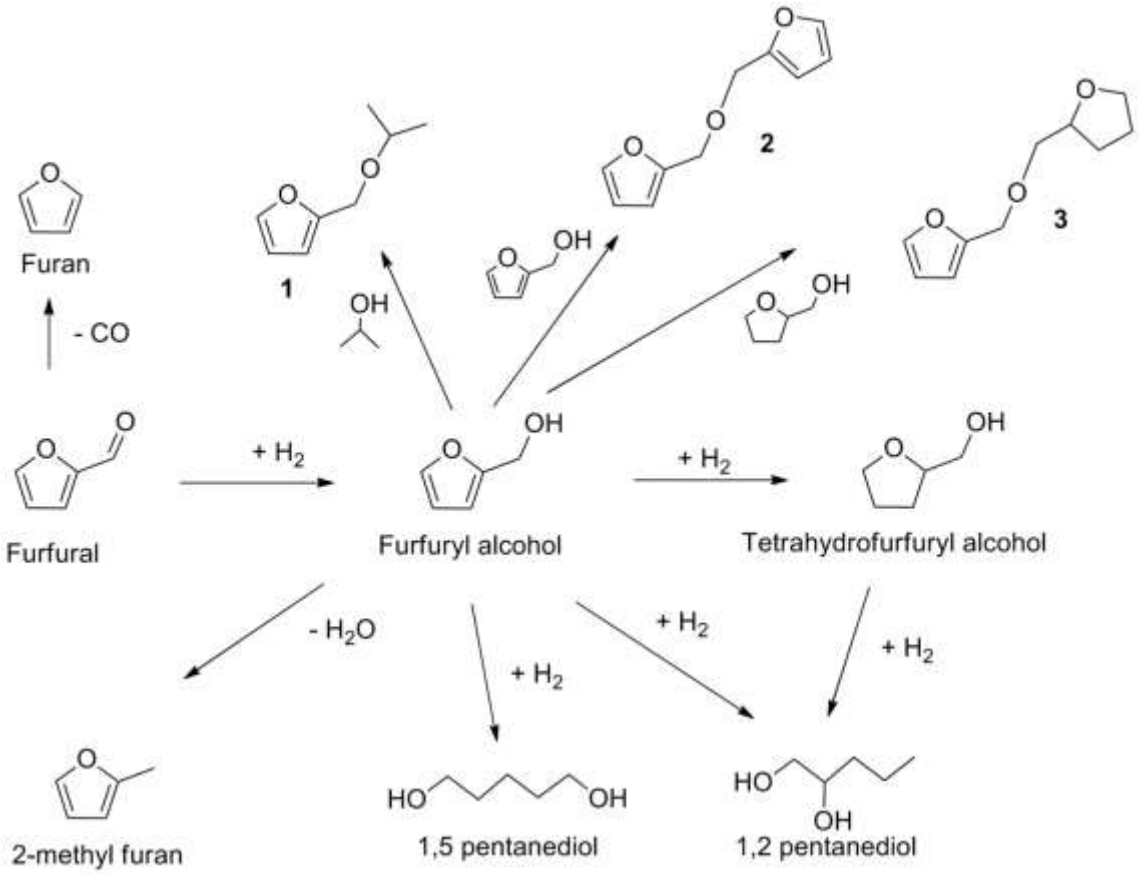

Scheme 1 Product distribution from reductive conversion of furfural

2. Experimental

2.1. Synthesis of MXenes

Multilayered Nb_2CT_x and $Nb_4C_3T_x$ MXenes were obtained by hydrofluoric acid (HF) etching of Al layers from MAX phases (Nb_2AlC and Nb_4AlC_3, respectively).

2.1.1 Synthesis of MAX phases

MAX phase powders were synthesized by mixing powders of niobium, Nb (Alfa Aesar, Ward Hill, USA, 99.9% purity, −325 mesh), aluminum, Al (Alfa Aesar, Ward Hill, USA, 99.5 wt.% purity; -325 mesh), and graphite, C (Alfa Aesar, Ward Hill, USA, 99 wt.% purity; - 300 mesh) in an atomic ratio of 2Nb : 1.3Al : 1C for Nb_2AlC, and 4Nb : 1.5Al : 2.7C for Nb_4AlC_3 for 3 h at 56 rpm in a Turbula T2F mixer with yttria-stabilized zirconia balls as mixing media. The mixture was then heated in a tube furnace for 4 h at 1600 °C with a 10 °C heating rate (or 5 °C/min) under a flow of argon for Nb_2AlC, while, for Nb_4AlC_3, powders were pressed into ca. 10 g pellets and heated at 1700 °C for 1 h with a 10 °C heating rate in a tube furnace under flowing argon. After the thermal cycle and cooling back to room temperature, the products were ground using a titanium-nitride-coated milling bit and sieved to -400 mesh.

2.1.2 HF etching

The sieved Nb_2AlC or Nb_4AlC_3 powders were stirred for 96 h at 40 °C after immersing in 50% HF aqueous solution. The resulting reaction mixtures were washed 6 times using deionized water and centrifuged at 3500 rpm to separate the MXenes as settled powders from the supernatants. After washing, the powders were dried using vacuum-assisted filtration at room temperature.

2.2. Characterization

X-ray diffraction patterns were collected using a Rigaku Cu K_α diffractometer (Rigaku Smart Lab, USA). Scanning steps of 0.02° 2Theta, and 1 s dwell time at each step were used.

X-ray photoelectron spectroscopy (XPS) data were collected using VG Scientific Mark II equipment, UK, with Al K_α (hν=1486.6eV) as excitation source. The surfaces of the samples were cleaned by Ar^+ sputtering for 5 minutes before collecting the spectra. The data were deconvoluted using the commercial CasaXPS software. Metal leaching was checked by ICP analysis on the solution after reaction after filtration of the solid catalyst, on a JobinYvon JY24.

Surface acid sites of $Nb_4C_3T_x$ and Nb_2CT_x samples were measured by titration in solid-liquid phase with solutions of 2-phenylethylamine (PEA, pK_a = 9.84) as the basic probe. Titrations were carried out in a modified liquid-chromatographic line operating in a recirculating mode, at 30.0°C±0.1°C in cyclohexane, an apolar/aprotic solvent, for the *intrinsic acidity* (I.A.) and in water:isopropanol mixture (50:50 v/v), a polar/protic solvent, for the *effective acidity* (E.A.).

Nb-containing samples (ca. 0.04 g, 80-200 mesh particles) were placed in a sample holder (stainless steel tube, 2 mm diameter and 12 cm of length) between two sand pillows. Samples underwent then thermal pre-treatment (150 °C in 8 mL min^{-1} air flux for 16 h) and successively the tube was filled with the solvent (cyclohexane or H_2O – 2-propanol mixture). The sample holder was then mounted on a recirculation chromatographic line (HPLC), equipped with a Waters 515 pump and a monochromatic UV detector (Waters, model 2487, working at fixed λ = 254 nm). During the analyses, the sample was maintained at constant temperature. By means of successive injections of dosed amounts of PEA (50 µL, ca. 0.10 M) into the line, a step-chromatogram was obtained, where each step represents the achieving of the probe adsorption equilibrium in the given liquid. After the collection of the first adsorption isotherm on fresh sample (I° run), pure solvent was flowed through the saturated sample overnight (ca. 16 h), thus permitting desorption of the probe molecules from weakly interacting sites; then, a new adsorption of PEA on the same sample was repeated (II° run) to quantify strong acid sites. Previous tests of PEA adsorptions on sea sand showed that the probe molecules were adsorbed in negligible amount. The collected isotherms were interpreted following the Langmuir model (equation 1):

$$\frac{PEA_{ads}}{PEA_{ads,max}\dfrac{b_{ads}[PEA]_{eq}}{\left(1+b_{ads}[PEA]_{eq}\right)}} \quad (1)$$

where, PEA_{ads} and $PEA_{ads,max}$ indicate the amount of PEA adsorbed and the maximum amount of PEA adsorbed by the surface, $[PEA]_{eq}$ indicates the PEA concentration in solution at equilibrium, and b_{ads} is the Langmuir constant. From the conventional linearized equation, reporting $[PEA]_{eq}/[PEA]_{ads}$ *vs*. $[PEA]_{eq}$, the values of $PEA_{ads,max}$ ($mmol \cdot g^{-1}$) could be obtained. Assuming a 1:1 stoichiometry for the PEA adsorption on the acid site, the value of $PEA_{ads,max}$ of the I run isotherm gives the total number of acid sites, while the value of $PEA_{ads,max}$ obtained from the II run isotherm corresponded to the number of weak acidic sites. The number of strong acid sites was obtained by the difference between the number of total and weak sites.

2.3. Catalytic tests

Furfural, F, (purity 99%, Sigma-Aldrich) hydrogenation was performed at 160 °C, in batch conditions in a stainless-steel reactor (0.030 L capacity), equipped with heater, mechanical stirrer, gas supply system and thermometer. Furfural solution (0.015 L; 0.3 M in 2-propanol) was added into the reactor and the desired amount of catalyst (F:catalyst ratio=50:50 wt) was suspended in the solution. The reactor was closed and pressurized at 5 bar (by nitrogen gas for CTH tests or hydrogen gas for direct hydrogenation tests). The mixture was heated to the reaction temperature, 160 °C, and mechanically stirred (1250 rpm). At the end of the reaction, the autoclave was cooled down. Samples were removed periodically (0.2 mL) and HP 7820A gas chromatograph equipped with a capillary column HP-5 30m x 0.32mm, 0.25 μm Film, by Agilent Technologies. For the identification and quantification of reagents and products, authentic samples were analyzed, and corresponding retention time and response factor were determined. External standard method (with 1-octanol as standard) was used for quantitative analysis.

For recycling tests, the CTH catalytic activity was tested over several runs. Each run was performed under the following reaction conditions: Furfural 0.3 M, and the catalyst (substrate:catalyst ratio = 50:50

wt, 4h) 5 bar N_2, 160 °C. The catalyst was recovered by filtration and re-used without any further treatment.

The catalytic behavior of Nb_2O_5 was also evaluated for the sake of comparison. $Nb_2O_5.nH_2O$ (with nominal composition 80 wt% Nb_2O_5 and 20 wt% H_2O, code AD/5260) powder sample was kindly supplied from Companhia Brasileira de Metalurgia e Mineração (CBMM, Brazil). All the hereinafter reported characterization data were from Ref. [52].

3. Results and discussion

Nb_2CT_x and $Nb_4C_3T_x$ MXenes were produced by selectively etching the Al layers in the parent MAX phases (Nb_2AlC and Nb_4AlC_3, respectively) using HF (Fig. 1a). This procedure yielded crystalline multilayered Nb- based MXenes, as demonstrated by XRD analysis. Indeed, the comparison between diffractograms of the powders obtained after HF etching (Fig. 1b and 1c, black curves) and the reference patterns of pristine MAX phases (ICSD 606236 and ICSD 160755 for Nb_2AlC and Nb_4AlC_3, respectively)[53] proved the successful formation of MXenes. Most of the peaks associated with the MAX phases either vanished completely or were significantly attenuated in intensity in the experimental diffractograms of Fig.1. The (002) peak decreased in intensity and broadened, and its position underwent a considerable downshift, indicative of an increase in the *c*-lattice parameters (*c*-LPs) as a consequence of an expansion along the [000*l*] direction. Such an expansion has been typically observed in MXenes, caused by the intercalation of water molecules in the intralayer space of MXenes. Specifically, the (0002) peak, that usually in Nb_2AlC occurs at 2θ of 12.7° (*c*-LP of 1.39 nm), is shifted at 2θ values of 7.9° (*c*-LP of 2.24 nm) in Nb_2CT_x, indicating a 0.85 nm expansion along the [000*l*]. Similarly, a downshift from a 2θ of 7.2° (*c*-LP of 2.24 nm) to 2θ of 6.2° (*c*-LP of 2.85 nm) was observed in (002) peak of $Nb_4C_3T_x$ sample, corresponding to more than 0.6 nm expansion along the [000*l*].

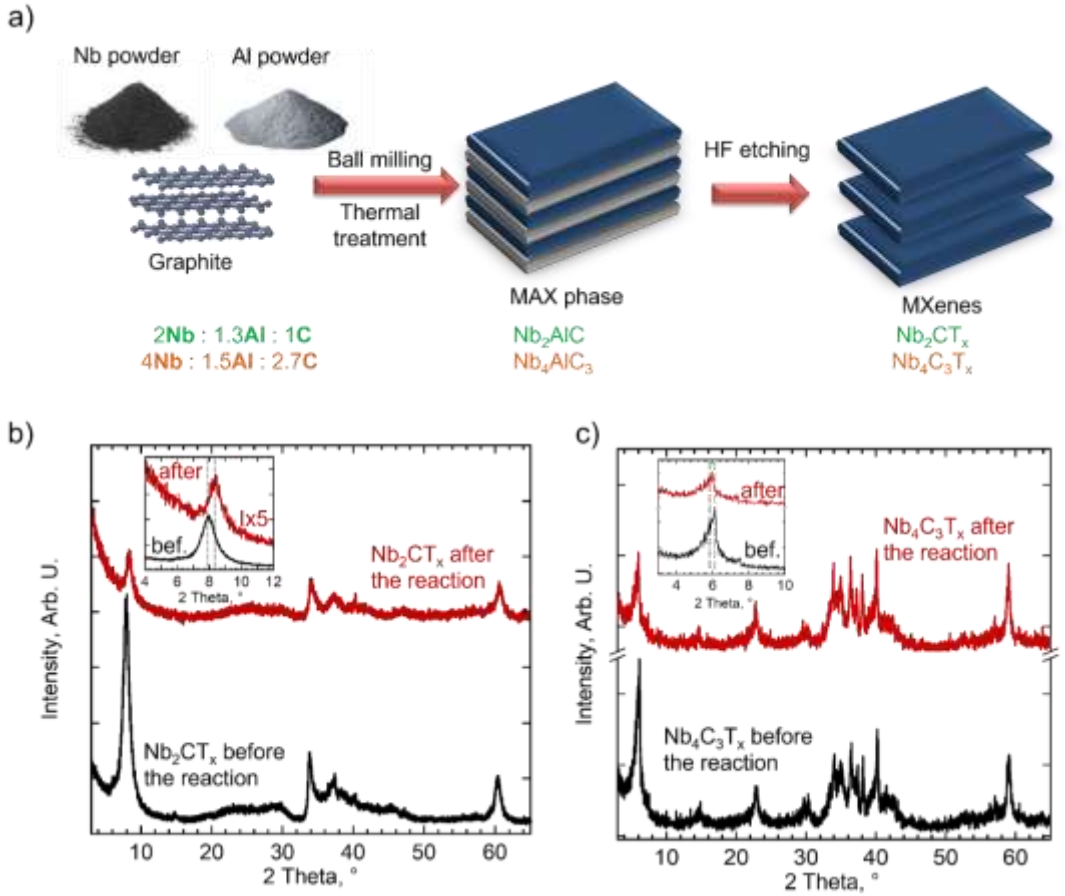

Fig. 1 a) schematic representation of Nb MXenes synthesis and XRD patterns of b) Nb_2CT_x and c) $Nb_4C_3T_x$ before and after the hydrogenation reaction.

Nb_2CT_x and $Nb_4C_3T_x$ were explored as catalysts for the catalytic transfer hydrogenation (CTH) of furfural using 2-propanol as hydrogen source in a liquid-phase batch process.

Table 1 Comparison of Nb-MXenes and Nb_2O_5 in the furfural hydrogenation in 2-propanol

Catalyst[a]	Activity[b]	Conversion after 8 h (%)	Selectivity[c] (%)							
			FA	THFA	2-MF	Ethers			1,2 PD	1,5 PD
						1	2	3		
Nb_2CT_x	130	57	28.4	0.0	3.2	50.1	16.8	-	-	-
$Nb_4C_3T_x$	73	70	18.6	0.3	6.0	51.8	21.9	-	-	-
Nb_2O_5	21	15	18.3[d]	2.5[d]	-	70.3[d]	1.5[d]	-	1.5[d]	-

[a] Reaction conditions: T = 160°C, batch conditions, furfural 0.3 M in 2-propanol, substrate/catalyst ratio=50 wt/wt; $p(N_2)$ = 5 bar.

[b] Converted $mmol_{furfural}\ g_{catalyst}^{-1}\ h^{-1}$, calculated after 1 h of reaction

[c] Selectivity at isoconversion (50%)

[d] Selectivity at 15% of conversion

The main results are summarized in Table 1 and demonstrate that Nb-MXenes were active for CTH of furfural. In particular, comparing the catalytic activity, defined as the furfural conversion rate per unit mass of catalyst (mols of converted furfural per grams of catalyst per time), over the first hour of the reaction time, Nb_2CT_x resulted to be almost twice as active as $Nb_4C_3T_x$ (130 versus 73 mol g^{-1} h^{-1}, respectively). The catalytic activity of commercial niobium oxide catalyst (Nb_2O_5 from CBMM) was also evaluated as a reference. Niobium oxide possessed poor activity (21 mol g^{-1} h^{-1}) in the studied reactions, reaching a conversion of only 15% after 8 h, in agreement with previous reports in the literature. [51] In general, from the comparison with data from Table S.1, Nb-MXenes emerge as highly active catalysts with superior activity compared to most noble metal-free catalysts already proposed in the literature. In particular, the Nb-MXenes exhibited higher activity than the Ti-MXenes (Table S.1, entries 4 and 5), thus highlighting the important role of Nb Lewis acid centers in the reaction.

On the other hand, the observed trend in catalytic activity the Nb-based catalysts studied here (Nb_2CT_x > $Nb_4C_3T_x$ >>Nb_2O_5) suggests that difference in the nature of Nb active sites or in the number of sites also play a crucial role, as discussed below.

Interestingly, looking at conversion data in Table 1, it is worth noting that after 8 h the highest furfural conversion (70%) was achieved over $Nb_4C_3T_x$, while slightly lower conversion (57%) was observed for Nb_2CT_x despite its higher initial activity. The loss over time of catalytic activity for Nb_2CT_x appears even more evident from conversion versus time plots in Fig.2 a. Although furfural conversion continuously increases with reaction time over Nb_2CT_x, after 4 h a significant decline in the slope of the curve can be observed. On the contrary the red curve, related to $Nb_4C_3T_x$, shows a close to linearly increasing trend with almost constant slope over the whole-time interval. Therefore, a comparative view of curves in Fig.2a suggests that Nb_2CT_x underwent deactivation in a larger extent than $Nb_4C_3T_x$. This tendency was confirmed by the results of stability tests carried out on Nb_2CT_x and $Nb_4C_3T_x$ catalysts (Fig.2 b and 2c respectively).

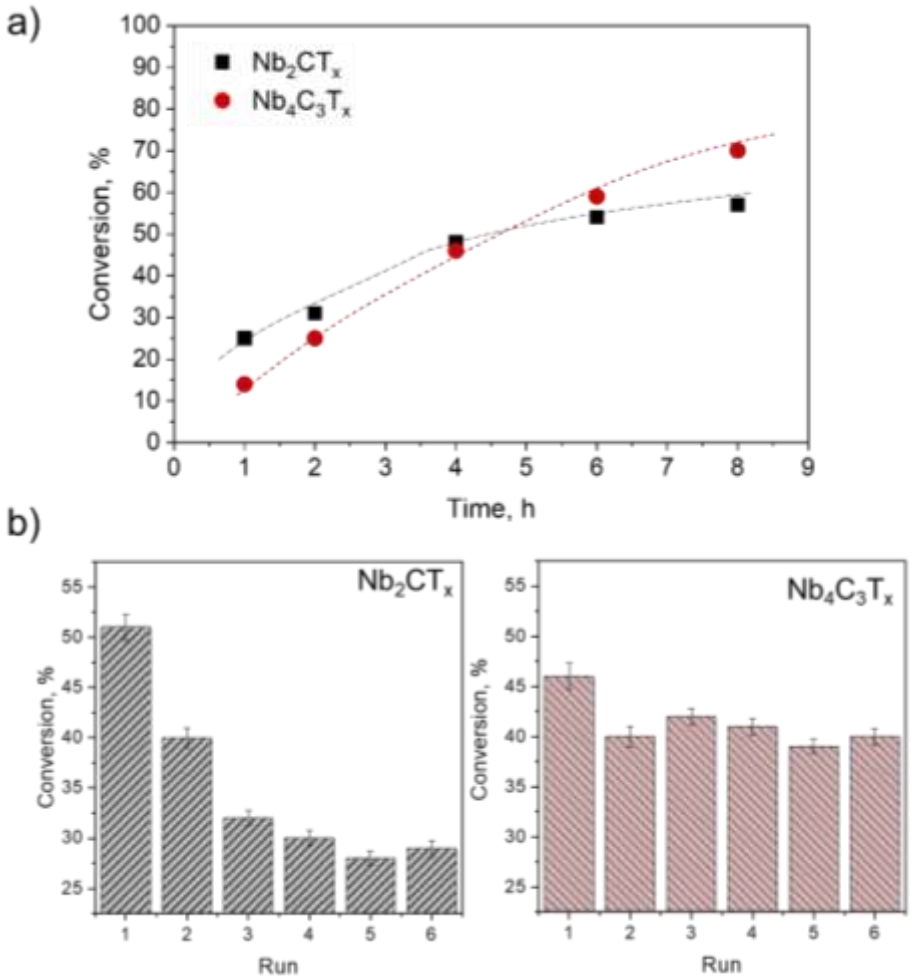

Fig.2 a) Conversion *vs.* time for Nb_2CT_x and $Nb_4C_3T_x$ and stability tests for b) Nb_2CT_x and c) $Nb_4C_3T_x$ (Reaction conditions: T = 160°C, batch conditions, furfural 0.3 M in 2-propanol, substrate/catalyst ratio=50 wt/wt; $p(N_2)$ = 5 bar, t = 8 h).

The stability of the catalysts was assessed by recycling experiments on catalyst grains, recovered by filtration and reused without any further purification over six runs. The catalytic activity of Nb_2CT_x significantly decreased through the first four consecutive reaction runs, reaching approximately 30% furfural conversion in the fifth and sixth reaction runs. XRD pattern of used catalyst (Figure 1b, red curve) revealed that MXene peaks were preserved with only small changes in intensity and in *c*-LP. In particular, the (002) peak of used Nb_2CT_x was shifted at higher angle (2θ of 8.4º) that corresponds to *c*-LP of ~ 2.10 nm, which is slightly lower than the pristine value (2.24 nm). It is known that the *c*-LP value

depends on the nature of the surface terminations,[54] and the intercalated species, if any.[55] Thus, the observed slight decrease of interlayer spacing of used Nb_2CT_x could be ascribed to a variation in the distribution of terminations after testing.

On the contrary, $Nb_4C_3T_x$ maintained good activity over six runs, except a marginal drop in the conversion between the first and second run, thus demonstrating to be an active and reusable catalyst. Indeed, both XRD pattern (Fig. 1c) and SEM (Fig.S.1) analyses on fresh and used samples confirmed that no relevant structural or morphological changes were observed after testing.

The comparison of product distributions of Nb_2CT_x and $Nb_4C_3T_x$ at iso-conversion (25%) showed only slight differences in the selectivity of the two catalysts (Table 1). Interestingly the presence of furfuryl alcohol and 2-methylfuran (the latter deriving from hydrogenolysis of the former) among the reaction products proved that Nb-MXenes were active in catalyzing the reduction of furfural through Meerwein Schmidt Ponndorf Verley Oppenauer (MPV) reaction. $Nb_4C_3T_x$ demonstrated its activity to promote the consecutive hydrogenolysis of FA (18.6%) to 2-MF (6%) more than Nb_2CT_x (selectivity to FA and 2-MF of 28.4% and 3.2%, respectively). In any case, on both catalysts, the competing etherification of the MPV reaction product (FA) with 2-propanol to form 2-(isopropoxy)methyl furan (here indicated as Ether 1) or with another furfuryl alcohol molecule to obtain difurfuryl ether (Ether 2) was the preferential pathway at early stages of the reaction (ethers accounted for ca. 70% of detected products), when an acid catalyst is employed, in agreement with the literature [56–58]. More remarkable discrepancies in the selectivity of Nb_2CT_x and $Nb_4C_3T_x$ emerged as the reaction progressed. Indeed, by monitoring the selectivity as a function of furfural conversion (Fig.3), it is significant to remark that 1,2 pentanediol became the predominant product at furfural conversion higher than 50% over Nb_2CT_x catalyst (44% of selectivity to 1,2-PD at 60% conversion), while the same trend was not observed on $Nb_4C_3T_x$. This an important result, since the formation of 1,2-PD is rarely reported in the furfural CTH over transition metal-based systems (being in most cases FA and 2-MF the main products, see Table S.1). In particular

catalysts with high Lewis acidity as well as bifunctional catalysts containing acid-metal (or base-metal) dual sites have been proven to be the most effective and selective catalysts for furfural conversion to 1,2-PD [59–63]. The acid site activates the O of the furan ring while the metal site promotes the dissociation of hydrogen and the formation of active H species which then catalyze ring-opening hydrogenolysis. The formation of 1,2-PD under CTH conditions represents a relevant aspect, which deserves to be further investigated in future works.

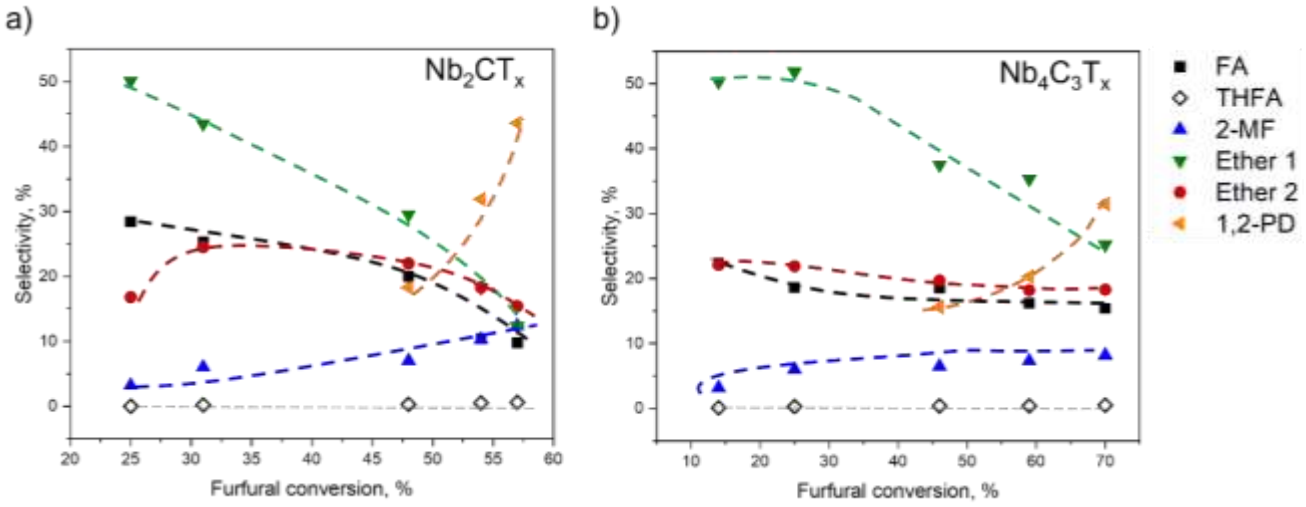

Fig.3 Selectivity *vs.* furfural conversion over a) Nb_2CT_x and b) $NB_4C_3T_x$

Targeted characterization of surface properties was carried out with the aim to better understand the origin of the observed difference in the activity, stability and selectivity of the samples and unravel the role of Nb active sites and surface acidity. Indeed, the Lewis acid character of catalyst surface has been recognized to be a key factor in determining the activity and selectivity in furfural CTH reaction. [64] Niobium materials, for their part, have been heavily investigated in the last decades because they have unique acid properties which are maintained even in the presence of polar and protic solvents.[46,65] Here, the acidity of Nb-based catalysts was quantitatively studied by solid-liquid phase titrations to fully ascertain the number of acid sites. The water tolerance of these materials was proven by comparing

results from titrations with 2-phenylethyl amine (PEA) basic probe in cyclohexane and in water/2-propanol mixture (50/50 v/v). Being cyclohexane an apolar-aprotic solvent unable to interact with any surface functionality, the intrinsic acidity (I.A.) of the sample surfaces was measured in this solvent. Differently, water/2-propanol mixture has been selected to simulate the polar environment of the catalytic tests and thus to assess the effective acidity (E.A.) manifested by the samples under reaction conditions. The obtained results have been gathered in Fig. 4, in which PEA adsorption isotherms (I° and II° runs described by full and empty symbols, respectively) collected in cyclohexane (top panels) and water/2-propanol (bottom panels) are reported. All the collected curves have asymptotic profiles with achievement of a plateau value for the adsorbed PEA, which corresponds to saturation of all surface acid sites. From the fitting of PEA adsorption isotherms by the Langmuir model equation the total number of acid sites could be deduced (Table 3). In addition, the percentage of strong acid sites was evaluated from the adsorption isotherm (red dotted curve), which represents the Langmuir curve of PEA adsorption on strong acid sites, calculated by comparing I° and II° runs adsorption on each sample.

Nb_2CT_x possessed higher *intrinsic acidity* (107 μequiv g^{-1}) in cyclohexane compared to $Nb_4C_3T_x$ (69 μequiv g^{-1}) and also larger proportion of strong acid sites (80% versus 54% of $Nb_4C_3T_x$). Interestingly, the acidity of Nb_2CT_x was maintained also in water/2-propanol mixture (100 μequiv g^{-1}), although the percentage of strong acid sites significantly decreased (from 80% to 25%). This confirmed the good tolerance of Nb materials towards polar and protic solvents, which weaken but do not suppress the acid character of Nb_2CT_x. A more pronounced drop in the acidity was observed for $Nb_4C_3T_x$ in polar protic medium (from 69 to 43 μequiv g^{-1}).

The larger amount of strong acid sites of Nb_2CT_x in the reaction environment could explain to some extent its higher initial activity compared to $Nb_4C_3T_x$. Furthermore, the presence of a large number of acid sites could also justify the higher propensity of Nb_2CT_x to deactivate. In fact, it is known that strong

acid sites promote condensation side-reactions which lead to the formation of polymers and solid deposits (humins), responsible for catalyst deactivation.[66]

On the other hand, the surface acidity cannot be the sole descriptor for the observed catalytic performances. Indeed, although pure Nb_2O_5 possesses four times greater number of effective acid sites than Nb_2CT_x, the latter is far more active (by factor 6.2) than the former.

Table 3 Surface acid site determined by solid-liquid phase titrations with PEA

	Acid site titrations by PEA[a]	
Catalyst	Intrinsic acidity (μequiv g^{-1})	Effective acidity (μequiv g^{-1})
Nb_2CT_x	107 (80%)[b]	100 (25%)[b]
$Nb_4C_3T_x$	69 (54%)[b]	43 (23%)[b]
Nb_2O_5[c]	572 (73%)[b]	382 (60%)[b]

[a] Adsorption temperature, 30 °C; solvent, cyclohexane for intrinsic acidity and water/2-propanol mixture for effective acidity measurements; measurements have been repeated and average accuracy was ± 5.6%

[b] Percent of strong acid sites.

[c] Data from Ref.[50]

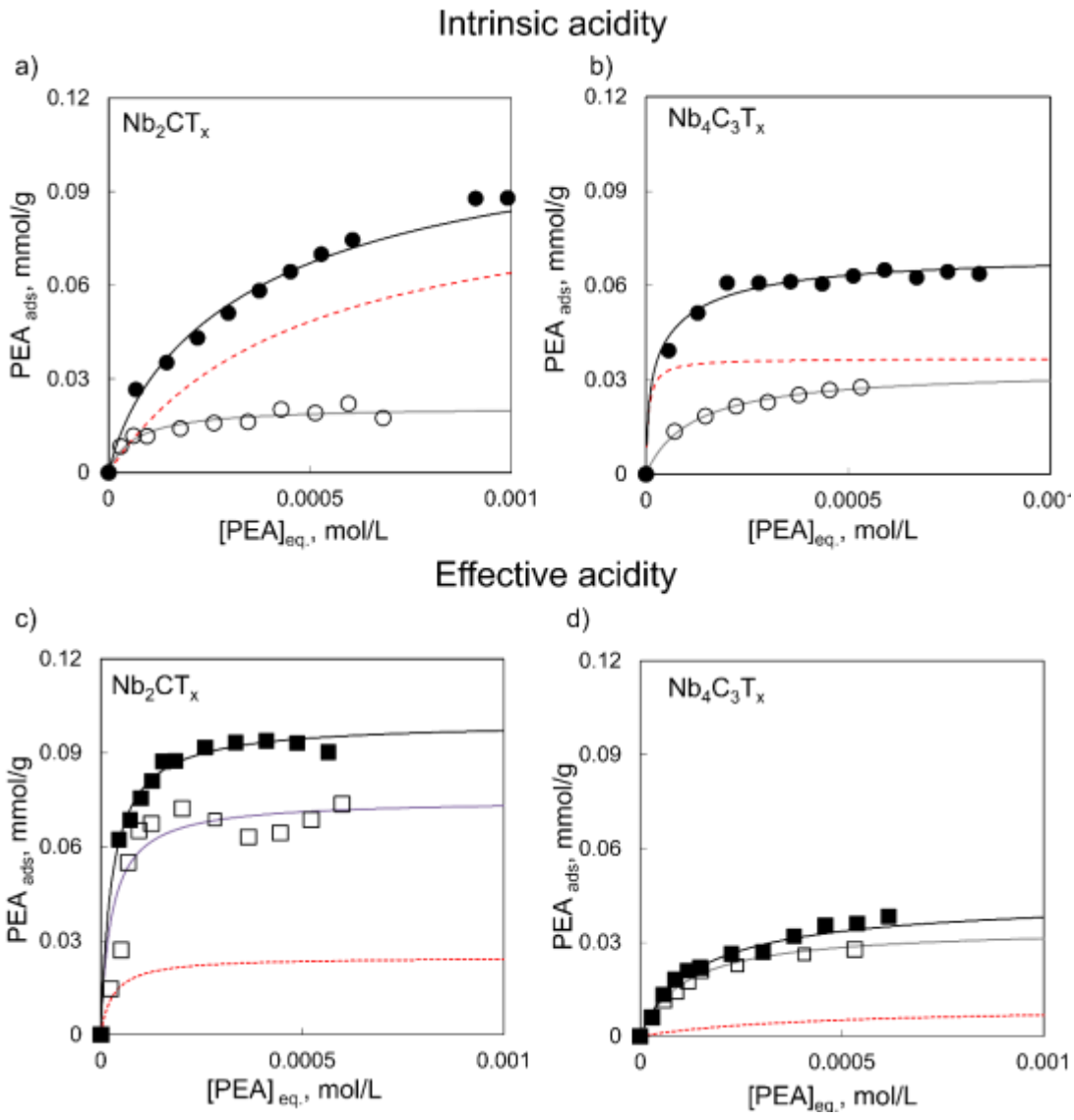

Fig 4 Adsorption isotherms at 30 °C of PEA probe on Nb-based samples evaluated in cyclohexane (a, b) for measuring the *intrinsic* acidity and in water-isopropanol solution (50:50 v/v), (c,d) for determining the *effective* acidity. Fitting Langmuir curves of I° run PEA adsorption (total acid sites), black lines and filled square markers; fitting Langmuir curves of the II° run PEA adsorption (weak acid sites), grey lines and empty square markers; calculated Langmuir of the strong acid sites, obtained from difference from the I° and II° PEA adsorptions, red dotted curves.

Actually, it is known that MXenes are characterized by a peculiar surface chemistry, which depends on several factors, such as the nature of terminations, aging time, the number of layers, as recently proved by X-ray photoelectron spectroscopy (XPS).[67]

XPS measurements were then carried out to analyze the chemical states of Nb and O before and after testing on $Nb_4C_3T_x$, while XPS characterization on Nb_2CT_x has been already reported in Ref. [68].

In the XPS survey scans of Nb_4C_3 MXenes before and after testing (Fig. S.2) Nb, C, F and O were detected. As exhibited in Fig. 5 a and b, in addition to surface oxides (Nb^{+1} to Nb^{+5}), Nb 3d was deconvoluted into three main species (Table S.2): (i) Nb near a C vacancy and interior Nb bond to only C without surface terminations ($Nb^{‡}$); (ii) Outer Nb bond to O and/or -OH (Nb^{*}); (iii) Outer Nb bond to F (C-Nb-F). The same spectral features were present in the XP spectrum of Nb_2CT_x, as recently published by some of the authors. [68] Furthermore, as summarized in Table S.3, it can be noticed that the three different Nb species deconvoluted and listed above have almost the same ratio in the used catalyst as before testing, indicating the chemical stability of $Nb_4C_3T_x$ MXene during testing. From O 1s spectra in Figure 6 c and d, we can observe that the most O come from the surface terminations (covering ~ 55-58%) and the surface terminations can keep stable before and after testing.

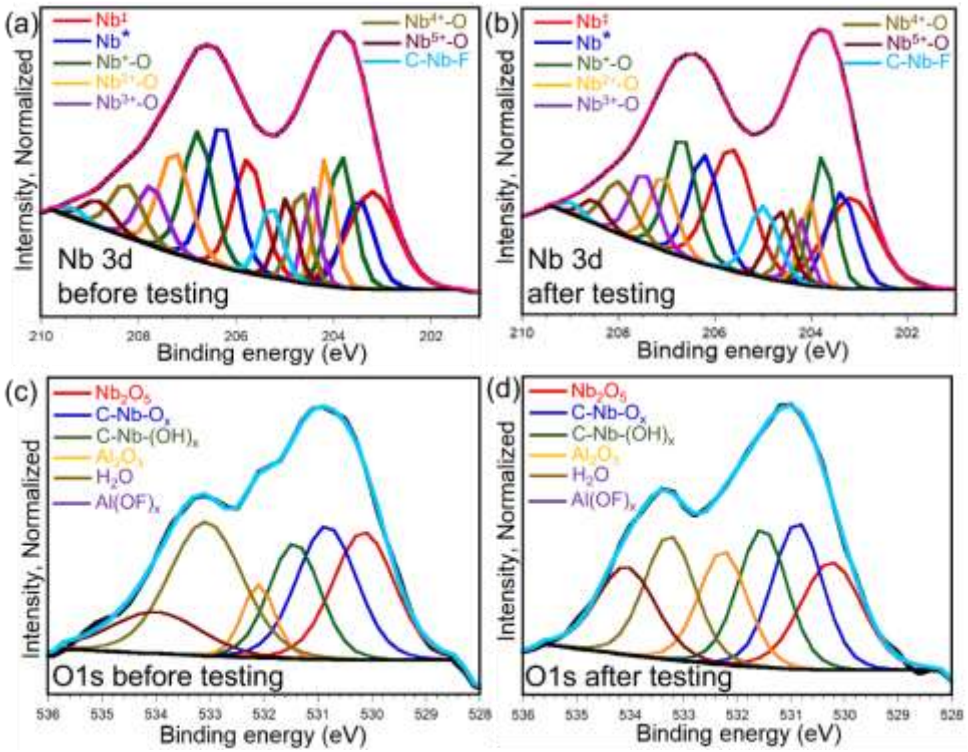

Fig. 5. XPS spectra of (a) Nb3d before testing (b) Nb3d after testing, (c) O1s before testing, (d) O1s after testing for $Nb_4C_3T_x$.

The presence of surface oxides (in particular Nb_2O_5) may impart the acid character to Nb-MXenes surfaces, which, similarly to pure Nb_2O_5, demonstrated to possess strong acid sites with good tolerance towards polar protic solvents. On the other hand, the characteristic unsaturated Nb species ($Nb^{‡}$, Nb^{*}, C – Nb – O and C-Nb-F) and surface terminations could be expected to confer unique reactivity to Nb-MXenes, thus explaining their higher activity compared to pure Nb_2O_5. In particular, thanks to their hydrogen affinity, – O terminations can serve as active sites for dehydrogenation reactions demonstrating to be active in the activation of C – H bond of organic molecules (*e.g.*, propane). The C–H activations proceeds through a radical-like pathway and leads to the formation of – OH terminal groups. The – O terminations are then restored by transformation of two adjacent OH groups into water and the concurrent associative desorption of H_2. [69]

Based on this evidence, a concerted mechanism involving Lewis acid sites and surface terminations could be proposed (Scheme 2).

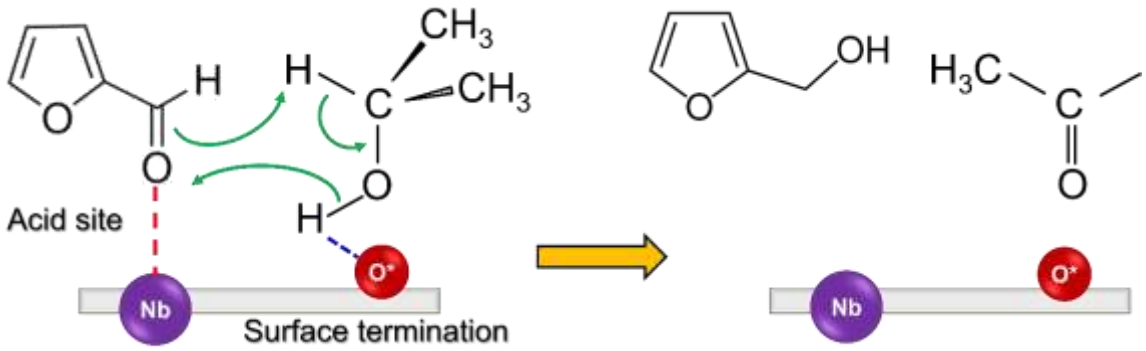

Scheme 2 Proposed mechanism for CTH

4. Conclusions

Nb-based MXenes (*viz.*, Nb_2CT_x and $Nb_4C_3T_x$) were successfully used as catalysts for the catalytic transfer hydrogenation of furfural. Both Nb_2CT_x and $Nb_4C_3T_x$ showed interesting activity and emerged as promising metal-free catalysts for biomass valorization reactions. The acid character of surfaces, ascribable to the presence of Nb_2O_5 clusters, could cause the enhanced activity of the studied catalysts. On the other hand, the presence of characteristic surface terminations also plays a key role in determining the unprecedented catalytic behavior of MXene phases.

The relevance of the collected observations represents an undoubtful incentive to pursue these studies with the aim to optimize the design of noble metal-free catalysts for the upgrading of biomasses.

References

[1] H. Xia, C. Chen, P. Liu, M. Zhou, J. Jiang, Selective hydrogenation of furfural for high-value chemicals: effect of catalysts and temperature, Sustain. Energy Fuels. 4 (2020) 5709–5720. https://doi.org/10.1039/d0se01090a.

[2] P. Khemthong, C. Yimsukanan, T. Narkkun, A. Srifa, T. Witoon, S. Pongchaiphol, S. Kiatphuengporn, K. Faungnawakij, Advances in catalytic production of value-added biochemicals and biofuels via furfural platform derived lignocellulosic biomass, Biomass and Bioenergy. 148 (2021) 106033. https://doi.org/10.1016/j.biombioe.2021.106033.

[3] K. Xiong, J.G. Chen, Correlating furfural reaction pathways with interactions between furfural and monometallic surfaces, Catal. Today. 339 (2020) 289–295. https://doi.org/10.1016/j.cattod.2018.10.004.

[4] O'Driscoll, J.J. Leahy, T. Curtin, The influence of metal selection on catalyst activity for the liquid phase hydrogenation of furfural to furfuryl alcohol, Catal. Today. 279 (2017) 194–201. https://doi.org/10.1016/j.cattod.2016.06.013.

[5] T. Fovanna, S. Campisi, A. Villa, A. Kambolis, G. Peng, D. Rentsch, O. Kröcher, M. Nachtegaal, D. Ferri, Ruthenium on phosphorous-modified alumina as an effective and stable catalyst for catalytic transfer hydrogenation of furfural, RSC Adv. 10 (2020) 11507–11516. https://doi.org/10.1039/d0ra00415d.

[6] S. Campisi, C.E. Chan-Thaw, L.E. Chinchilla, A. Chutia, G.A. Botton, K.M.H. Mohammed, N. Dimitratos, P.P. Wells, A. Villa, Dual-Site-Mediated Hydrogenation Catalysis on Pd/NiO: Selective Biomass Transformation and Maintenance of Catalytic Activity at Low Pd Loading, ACS Catal. 10 (2020) 5483–5492. https://doi.org/10.1021/acscatal.0c00414.

[7] Y. Wang, D. Zhao, D. Rodríguez-Padrón, C. Len, Recent Advances in Catalytic Hydrogenation of Furfural, Catalysts. 9 (2019) 796. https://doi.org/10.3390/catal9100796.

[8] S. Chen, R. Wojcieszak, F. Dumeignil, E. Marceau, S. Royer, How Catalysts and Experimental Conditions Determine the Selective Hydroconversion of Furfural and 5-Hydroxymethylfurfural,

Chem. Rev. 118 (2018) 11023–11117. https://doi.org/10.1021/acs.chemrev.8b00134.

[9] S. Campisi, D. Motta, I. Barlocco, R. Stones, T.W. Chamberlain, A. Chutia, N. Dimitratos, A. Villa, Furfural Adsorption and Hydrogenation at the Oxide-Metal Interface: Evidence of the Support Influence on the Selectivity of Iridium-Based Catalysts, ChemCatChem. n/a (2022) e202101700. https://doi.org/https://doi.org/10.1002/cctc.202101700.

[10] M.G. Quesne, A. Roldan, N.H. De Leeuw, C.R.A. Catlow, Bulk and surface properties of metal carbides: Implications for catalysis, Phys. Chem. Chem. Phys. 20 (2018) 6905–6916. https://doi.org/10.1039/c7cp06336a.

[11] K.J. Smith, Metal carbides, phosphides, and nitrides for biomass conversion, Curr. Opin. Green Sustain. Chem. 22 (2020) 47–53. https://doi.org/10.1016/j.cogsc.2019.11.008.

[12] C.E. Chan-Thaw, A. Villa, Metal carbides for biomass valorization, Appl. Sci. 8 (2018) 1–19. https://doi.org/10.3390/app8020259.

[13] J. Pang, J. Sun, M. Zheng, H. Li, Y. Wang, T. Zhang, Transition metal carbide catalysts for biomass conversion: A review, Appl. Catal. B Environ. 254 (2019) 510–522. https://doi.org/10.1016/j.apcatb.2019.05.034.

[14] P. Bretzler, M. Huber, A.A. Rane, R.E. Jentoft, K. Köhler, F.C. Jentoft, Selective synthesis of tungsten carbide phases W2C and WC as hydrogenation catalysts, J. Catal. 405 (2022) 60–73. https://doi.org/10.1016/j.jcat.2021.11.025.

[15] K. Xiong, W.S. Lee, A. Bhan, J.G. Chen, Molybdenum carbide as a highly selective deoxygenation catalyst for converting furfural to 2-methylfuran, ChemSusChem. 7 (2014) 2146–2149. https://doi.org/10.1002/cssc.201402033.

[16] W.S. Lee, Z. Wang, W. Zheng, D.G. Vlachos, A. Bhan, Vapor phase hydrodeoxygenation of

furfural to 2-methylfuran on molybdenum carbide catalysts, Catal. Sci. Technol. 4 (2014) 2340–2352. https://doi.org/10.1039/c4cy00286e.

[17] Z. Lin, W. Wan, S. Yao, J.G. Chen, Cobalt-modified molybdenum carbide as a selective catalyst for hydrodeoxygenation of furfural, Appl. Catal. B Environ. 233 (2018) 160–166. https://doi.org/10.1016/j.apcatb.2018.03.113.

[18] J.R. McManus, J.M. Vohs, Deoxygenation of glycolaldehyde and furfural on Mo2C/Mo(100), Surf. Sci. 630 (2014) 16–21. https://doi.org/10.1016/j.susc.2014.06.019.

[19] Y. Deng, R. Gao, L. Lin, T. Liu, X.D. Wen, S. Wang, D. Ma, Solvent Tunes the Selectivity of Hydrogenation Reaction over α-MoC Catalyst, J. Am. Chem. Soc. 140 (2018) 14481–14489. https://doi.org/10.1021/jacs.8b09310.

[20] I.N. Shilov, A.A. Smirnov, O.A. Bulavchenko, V.A. Yakovlev, Effect of Ni–Mo carbide catalyst formation on furfural hydrogenation, Catalysts. 8 (2018) 1–24. https://doi.org/10.3390/catal8110560.

[21] Y.B. Huang, M.Y. Chen, L. Yan, Q.X. Guo, Y. Fu, Nickel-tungsten carbide catalysts for the production of 2,5-dimethylfuran from biomass-derived molecules, ChemSusChem. 7 (2014) 1068–1072. https://doi.org/10.1002/cssc.201301356.

[22] M. Naguib, M.W. Barsoum, Y. Gogotsi, Ten Years of Progress in the Synthesis and Development of MXenes, Adv. Mater. 33 (2021) 2103393. https://doi.org/https://doi.org/10.1002/adma.202103393.

[23] M. Dadashi Firouzjaei, M. Karimiziarani, H. Moradkhani, M. Elliott, B. Anasori, MXenes: The two-dimensional influencers, Mater. Today Adv. 13 (2022) 100202. https://doi.org/10.1016/j.mtadv.2021.100202.

[24] T. Niu, Old materials with new properties II: The metal carbides, Nano Today. 18 (2018) 12–14. https://doi.org/10.1016/j.nantod.2017.10.001.

[25] Q. Fu, X. Bao, Surface chemistry and catalysis confined under two-dimensional materials, Chem. Soc. Rev. 46 (2017) 1842–1874. https://doi.org/10.1039/c6cs00424e.

[26] K.R.G. Lim, A.D. Handoko, S.K. Nemani, B. Wyatt, H.Y. Jiang, J. Tang, B. Anasori, Z.W. Seh, Rational Design of Two-Dimensional Transition Metal Carbide/Nitride (MXene) Hybrids and Nanocomposites for Catalytic Energy Storage and Conversion, ACS Nano. 14 (2020) 10834–10864. https://doi.org/10.1021/acsnano.0c05482.

[27] Y. Wu, X. Li, H. Zhao, F. Yao, J. Cao, Z. Chen, X. Huang, D. Wang, Q. Yang, Recent advances in transition metal carbides and nitrides (MXenes): Characteristics, environmental remediation and challenges, Chem. Eng. J. 418 (2021) 129296. https://doi.org/10.1016/j.cej.2021.129296.

[28] M. Naguib, J. Halim, J. Lu, K.M. Cook, L. Hultman, Y. Gogotsi, M.W. Barsoum, New two-dimensional niobium and vanadium carbides as promising materials for li-ion batteries, J. Am. Chem. Soc. 135 (2013) 15966–15969. https://doi.org/10.1021/ja405735d.

[29] M. Naguib, V.N. Mochalin, M.W. Barsoum, Y. Gogotsi, 25th anniversary article: MXenes: A new family of two-dimensional materials, Adv. Mater. 26 (2014) 992–1005. https://doi.org/10.1002/adma.201304138.

[30] Y.W. Cheng, J.H. Dai, Y.M. Zhang, Y. Song, Two-Dimensional, Ordered, Double Transition Metal Carbides (MXenes): A New Family of Promising Catalysts for the Hydrogen Evolution Reaction, J. Phys. Chem. C. 122 (2018) 28113–28122. https://doi.org/10.1021/acs.jpcc.8b08914.

[31] Á. Morales-Garciá, F. Calle-Vallejo, F. Illas, MXenes: New Horizons in Catalysis, ACS Catal. 10 (2020) 13487–13503. https://doi.org/10.1021/acscatal.0c03106.

[32] Z. Li, L. Yu, C. Milligan, T. Ma, L. Zhou, Y. Cui, Z. Qi, N. Libretto, B. Xu, J. Luo, E. Shi, Z. Wu, H. Xin, W.N. Delgass, J.T. Miller, Y. Wu, Two-dimensional transition metal carbides as supports for tuning the chemistry of catalytic nanoparticles, Nat. Commun. 9 (2018) 1–8. https://doi.org/10.1038/s41467-018-07502-5.

[33] Y. Liu, H. Gao, Y. Zhu, S. Li, J. Zhang, L. Li, Excellent catalytic activity of a two-dimensional Nb4C3Tx (MXene) on hydrogen storage of MgH2, Appl. Surf. Sci. 493 (2019) 431–440. https://doi.org/10.1016/j.apsusc.2019.07.037.

[34] Q. Zhu, Y. Cui, Y. Zhang, Z. Cao, Y. Shi, J. Gu, Z. Du, B. Li, S. Yang, Strategies for engineering the MXenes toward highly active catalysts, Mater. Today Nano. 13 (2021). https://doi.org/10.1016/j.mtnano.2020.100104.

[35] H. Oschinski, Á. Morales-García, F. Illas, Interaction of First Row Transition Metals with M2C (M = Ti, Zr, Hf, V, Nb, Ta, Cr, Mo, and W) MXenes: A Quest for Single-Atom Catalysts, J. Phys. Chem. C. 125 (2021) 2477–2484. https://doi.org/10.1021/acs.jpcc.0c10877.

[36] K. Liang, A. Tabassum, M. Kothakonda, X. Zhang, R. Zhang, B. Kenney, B.D. Koplitz, J. Sun, M. Naguib, Two-dimensional titanium carbonitride MXene as a highly efficient electrocatalyst for hydrogen evolution reaction, Mater. Reports Energy. 2 (2022) 100075. https://doi.org/10.1016/j.matre.2021.100075.

[37] M. Naguib, W. Tang, K.L. Browning, G.M. Veith, V. Maliekkal, M. Neurock, A. Villa, Catalytic Activity of Ti-based MXenes for the Hydrogenation of Furfural, ChemCatChem. 12 (2020) 5733–5742. https://doi.org/10.1002/cctc.202000977.

[38] P. Carniti, A. Gervasini, M. Marzo, Silica-niobia oxides as viable acid catalysts in water: Effective vs. intrinsic acidity, Catal. Today. 152 (2010) 42–47.

https://doi.org/10.1016/j.cattod.2009.07.111.

[39] R.L. Martins, W.J. Schitine, F.R. Castro, Texture, surface acidic and catalytic properties of niobium phosphate, Catal. Today. 5 (1989) 483–491. https://doi.org/10.1016/0920-5861(89)80012-4.

[40] C. García-Sancho, J.M. Rubio-Caballero, J.M. Mérida-Robles, R. Moreno-Tost, J. Santamaría-González, P. Maireles-Torres, Mesoporous Nb2O5 as solid acid catalyst for dehydration of d-xylose into furfural, Catal. Today. 234 (2014) 119–124. https://doi.org/10.1016/j.cattod.2014.02.012.

[41] K. Tanabe, Catalytic application of niobium compounds, Catal. Today. 78 (2003) 65–77. https://doi.org/10.1016/S0920-5861(02)00343-7.

[42] I.E. Wachs, J.M. Jehng, G. Deo, H. Hu, N. Arora, Redox properties of niobium oxide catalysts, Catal. Today. 28 (1996) 199–205. https://doi.org/10.1016/0920-5861(95)00229-4.

[43] M. Ziolek, Niobium-containing catalysts - The state of the art, Catal. Today. 78 (2003) 47–64. https://doi.org/10.1016/S0920-5861(02)00340-1.

[44] P. Carniti, A. Gervasini, S. Biella, A. Auroux, Niobic acid and niobium phosphate as highly acidic viable catalysts in aqueous medium: Fructose dehydration reaction, Catal. Today. 118 (2006) 373–378. https://doi.org/10.1016/j.cattod.2006.07.024.

[45] S. Kang, R. Miao, J. Guo, J. Fu, Sustainable production of fuels and chemicals from biomass over niobium based catalysts: A review, Catal. Today. 374 (2021) 61–76. https://doi.org/10.1016/j.cattod.2020.10.029.

[46] M. Ziolek, I. Sobczak, The role of niobium component in heterogeneous catalysts, Catal. Today. 285 (2017) 211–225. https://doi.org/10.1016/j.cattod.2016.12.013.

[47] M.J.C. Molina, M.L. Granados, A. Gervasini, P. Carniti, Exploitment of niobium oxide effective acidity for xylose dehydration to furfural, Catal. Today. 254 (2015) 90–98. https://doi.org/10.1016/j.cattod.2015.01.018.

[48] J.C. Védrine, G. Coudurier, A. Ouqour, P.G. Pries De Oliveira, J.C. Volta, Niobium oxide based materials as catalysts for acidic and partial oxidation type reactions, Catal. Today. 28 (1996) 3–15. https://doi.org/10.1016/0920-5861(95)00213-8.

[49] J.R.H. Ross, R.H.H. Smits, K. Seshan, The use of niobia in oxidation catalysis, Catal. Today. 16 (1993) 503–511. https://doi.org/10.1016/0920-5861(93)80091-E.

[50] S. Campisi, S. Bennici, A. Auroux, P. Carniti, A. Gervasini, A Rational Revisiting of Niobium Oxophosphate Catalysts for Carbohydrate Biomass Reactions, Top. Catal. 61 (2018) 1939–1948. https://doi.org/10.1007/s11244-018-0999-x.

[51] A. Jouve, S. Cattaneo, D. Delgado, N. Scotti, C. Evangelisti, J.M.L. Nieto, L. Prati, Furfural hydrogenation on modified niobia, Appl. Sci. 9 (2019). https://doi.org/10.3390/app9112287.

[52] M.N. Catrinck, S. Campisi, P. Carniti, R.F. Teófilo, F. Bossola, A. Gervasini, Phosphate enrichment of niobium-based catalytic surfaces in relation to reactions of carbohydrate biomass conversion: The case studies of inulin hydrolysis and fructose dehydration, Catalysts. 11 (2021). https://doi.org/10.3390/catal11091077.

[53] K.J. Griffith, M.A. Hope, P.J. Reeves, M. Anayee, Y. Gogotsi, C.P. Grey, Bulk and Surface Chemistry of the Niobium MAX and MXene Phases from Multinuclear Solid-State NMR Spectroscopy, J. Am. Chem. Soc. 142 (2020) 18924–18935. https://doi.org/10.1021/jacs.0c09044.

[54] N.M. Caffrey, Effect of mixed surface terminations on the structural and electrochemical

properties of two-dimensional Ti3C2T2 and V2CT2 MXenes multilayers, Nanoscale. 10 (2018) 13520–13530. https://doi.org/10.1039/c8nr03221a.

[55] O. Mashtalir, M. Naguib, V.N. Mochalin, Y. Dall'Agnese, M. Heon, M.W. Barsoum, Y. Gogotsi, Intercalation and delamination of layered carbides and carbonitrides, Nat. Commun. 4 (2013) 1–7. https://doi.org/10.1038/ncomms2664.

[56] P. Panagiotopoulou, N. Martin, D.G. Vlachos, Effect of hydrogen donor on liquid phase catalytic transfer hydrogenation of furfural over a Ru/RuO2/C catalyst, J. Mol. Catal. A Chem. 392 (2014) 223–228. https://doi.org/10.1016/j.molcata.2014.05.016.

[57] P. Panagiotopoulou, D.G. Vlachos, Liquid phase catalytic transfer hydrogenation of furfural over a Ru/C catalyst, Appl. Catal. A Gen. 480 (2014) 17–24. https://doi.org/10.1016/j.apcata.2014.04.018.

[58] G.F. Tierney, S. Alijani, M. Panchal, D. Decarolis, M.B. de Gutierrez, K.M.H. Mohammed, J. Callison, E.K. Gibson, P.B.J. Thompson, P. Collier, N. Dimitratos, E.C. Corbos, F. Pelletier, A. Villa, P.P. Wells, Controlling the Production of Acid Catalyzed Products of Furfural Hydrogenation by Pd/TiO2, ChemCatChem. n/a (2021). https://doi.org/https://doi.org/10.1002/cctc.202101036.

[59] P.P. Upare, Y. Kim, K.-R. Oh, S.J. Han, S.K. Kim, D.-Y. Hong, M. Lee, P. Manjunathan, D.W. Hwang, Y.K. Hwang, A Bimetallic Ru 3 Sn 7 Nanoalloy on ZnO Catalyst for Selective Conversion of Biomass-Derived Furfural into 1,2-Pentanediol , ACS Sustain. Chem. Eng. (2021). https://doi.org/10.1021/acssuschemeng.1c05322.

[60] D.S. Pisal, G.D. Yadav, Single-Step Hydrogenolysis of Furfural to 1,2-Pentanediol Using a Bifunctional Rh/OMS-2 Catalyst, ACS Omega. 4 (2019) 1201–1214.

https://doi.org/10.1021/acsomega.8b01595.

[61] N. Wang, Z. Chen, L. Liu, Acid catalysis dominated suppression of xylose hydrogenation with increasing yield of 1,2-pentanediol in the acid-metal dual catalyst system, Appl. Catal. A Gen. 561 (2018) 41–48. https://doi.org/10.1016/j.apcata.2018.05.019.

[62] B. Zhang, Y. Zhu, G. Ding, H. Zheng, Y. Li, Selective conversion of furfuryl alcohol to 1,2-pentanediol over a Ru/MnOx catalyst in aqueous phase, Green Chem. 14 (2012) 3402–3409. https://doi.org/10.1039/c2gc36270h.

[63] P. Bretzler, M. Huber, S. Nickl, K. Köhler, Hydrogenation of furfural by noble metal-free nickel modified tungsten carbide catalysts, RSC Adv. 10 (2020) 27323–27330. https://doi.org/10.1039/d0ra02003f.

[64] M.J. Gilkey, P. Panagiotopoulou, A. V. Mironenko, G.R. Jenness, D.G. Vlachos, B. Xu, Mechanistic Insights into Metal Lewis Acid-Mediated Catalytic Transfer Hydrogenation of Furfural to 2-Methylfuran, ACS Catal. 5 (2015) 3988–3994. https://doi.org/10.1021/acscatal.5b00586.

[65] T. Okuhara, Water-tolerant solid acid catalysts, Chem. Rev. 102 (2002) 3641–3666. https://doi.org/10.1021/cr0103569.

[66] R. Weingarten, G.A. Tompsett, W.C. Conner, G.W. Huber, Design of solid acid catalysts for aqueous-phase dehydration of carbohydrates: The role of Lewis and Brønsted acid sites, J. Catal. 279 (2011) 174–182. https://doi.org/10.1016/j.jcat.2011.01.013.

[67] J. Halim, K.M. Cook, M. Naguib, P. Eklund, Y. Gogotsi, J. Rosen, M.W. Barsoum, X-ray photoelectron spectroscopy of select multi-layered transition metal carbides (MXenes), Appl. Surf. Sci. 362 (2016) 406–417. https://doi.org/10.1016/j.apsusc.2015.11.089.

[68] T. Su, R. Peng, Z.D. Hood, M. Naguib, I.N. Ivanov, J.K. Keum, Z. Qin, Z. Guo, Z. Wu, One-Step Synthesis of Nb2O5/C/Nb2C (MXene) Composites and Their Use as Photocatalysts for Hydrogen Evolution, ChemSusChem. 11 (2018) 688–699. https://doi.org/10.1002/cssc.201702317.

[69] K. Niu, L. Chi, J. Rosen, J. Björk, C-H activation of light alkanes on MXenes predicted by hydrogen affinity, Phys. Chem. Chem. Phys. 22 (2020) 18622–18630. https://doi.org/10.1039/d0cp02471f.

Supporting information

Table S.1 Literature overview on catalytic performances of noble metal-free catalysts for reductive conversion of furfural

Catalyst	T (°C)	Pressure (bar), gas	FA/catalyst ratio wt/wt	Activity [a]	Conversion (%)	Selectivity (%)		Ref
						FA	2-MF	
Nb_2CT_x	160	5, N_2	50	130 (1 h)	57 (8 h)	10	12	This work
$Nb_4C_3T_x$	160	5, N_2	50	73 (1 h)	70 (8 h)	15	8	This work
Ti_3CNT_z	180	5, N_2	50	72 (3 h)	46 (48 h)	49	17	[1]
$Ti_3C_2T_z$	180	5, N_2	50	88 (3 h)	38 (48 h)	52	10	[1]
MoC	150	3, H_2	6.6	15 (3 h)	97 (6 h)	10	89	[2]
Nb_2O_5	160	5, N_2	50	21 (1 h)	15 (8 h)	18	-	This work
TiO_2	150	1, N_2	3.2	10	29 (1 h)	57	-	[3]
NiO	150	1, N_2	3.2	18	54 (1 h)	97	-	[3]
MgO	120	0, H_2	2	0.3	3.6 (2 h)	15.1	n.d.	[4]
CaO	120	0, H_2	2	0.2	1.8 (2 h)	75.6	n.d.	[4]
SiO_2	120	0, H_2	2	2.1	19 (2 h)	2.9	n.d.	[4]
Al_2O_3	120	0, H_2	2	3.0	29.9 (2 h)	74.5	n.d.	[4]
HfO_2	120	0, H_2	2	3.3	32.5 (2 h)	85.5	n.d.	[4]
ZrO_2	120	0, H_2	2	2.8	28.3 (2 h)	83.4	n.d.	[4]

$70Al_2O_3$-$30ZrO_4$	120	autogenous	5	7.5 (0.5 h)	21.9	34.2	n.d.	[5]
Al_2O_3-ZrO_4-Fe_3O_4	180	autogenous	2.5	n.d.	93.6 (4 h)	86	n.d.	[5]
Co_3O_4/MC	160	1, N_2	2	401	>99 (4 h)	97	n.d.	[6]
PhP-Hf	140	n.d.	2	18.5 (1 h)	>99 (4 h)	96.5		[4]
Ni0.5MoC–SiO_2	150	60, H_2	3	7	n.d.	70	25	[7]
Cu/MgO−Al_2O_3	210	1, N_2	4	42	>99 (1 h)	90	-	[8]
Ni/SiO_2	80	34, H_2	10	2	10 (5 h)	49	-	[9]
Co/SiO_2	80	34, H_2	10	2	10 (5 h)	53	-	[9]
5%Ni/AC	260	autogenous	8	n.d.	95 (5 h)	19	48	[10]
5%Ni-15%W/AC	260	autogenous	8	n.d.	83 (5 h)	19	7	[11]
10%Ni-15%W/AC	260	autogenous	8	n.d.	83 (5 h)	30	7	[11]
$NiFe_2O_4$	220	n.d.	3	0.3	99 (6 h)	71	-	[12]
Fe_2O_3@HAP	180	10	2.4	1.0	96 (10 h)	95	-	[13]

[a] Activity (Converted $mmol_{furfural}\ g_{catalyst}^{-1}\ h^{-1}$)

[1] M. Naguib, W. Tang, K.L. Browning, G.M. Veith, V. Maliekkal, M. Neurock, A. Villa, Catalytic Activity of Ti-based MXenes for the Hydrogenation of Furfural, ChemCatChem. 12 (2020) 5733–5742. https://doi.org/10.1002/cctc.202000977.

[2] Y. Deng, R. Gao, L. Lin, T. Liu, X.D. Wen, S. Wang, D. Ma, Solvent Tunes the Selectivity of Hydrogenation Reaction over α-MoC Catalyst, J. Am. Chem. Soc. 140 (2018) 14481–14489. https://doi.org/10.1021/jacs.8b09310.

[3] J. He, L. Schill, S. Yang, A. Riisager, Catalytic Transfer Hydrogenation of Bio-Based Furfural with NiO Nanoparticles, ACS Sustain. Chem. Eng. 6 (2018) 17220–17229. https://doi.org/10.1021/acssuschemeng.8b04579.

[4] H. Li, Y. Li, Z. Fang, R.L. Smith, Efficient catalytic transfer hydrogenation of biomass-based furfural to furfuryl alcohol with recycable Hf-phenylphosphonate nanohybrids, Catal. Today. 319 (2019) 84–92. https://doi.org/10.1016/j.cattod.2018.04.056.

[5] J. He, H. Li, A. Riisager, S. Yang, Catalytic Transfer Hydrogenation of Furfural to Furfuryl Alcohol with Recyclable Al–Zr@Fe Mixed Oxides, ChemCatChem. 10 (2018) 430–438. https://doi.org/10.1002/cctc.201701266.

[6] G.-H. Wang, X. Deng, D. Gu, K. Chen, H. Tüysüz, B. Spliethoff, H.-J. Bongard, C. Weidenthaler, W. Schmidt, F. Schüth, Co 3 O 4 Nanoparticles Supported on Mesoporous Carbon for Selective Transfer Hydrogenation of α,β-Unsaturated Aldehydes , Angew. Chemie. 128 (2016) 11267–11271. https://doi.org/10.1002/ange.201604673.

[7] I. Shilov, A. Smirnov, O. Bulavchenko, V. Yakovlev, I.N. Shilov, A.A. Smirnov, O.A. Bulavchenko, V.A. Yakovlev, Effect of Ni–Mo Carbide Catalyst Formation on Furfural Hydrogenation, Catalysts. 8 (2018) 560. https://doi.org/10.3390/catal8110560.

[8] H. Chen, H. Ruan, X. Lu, J. Fu, T. Langrish, X. Lu, Efficient catalytic transfer hydrogenation of furfural to furfuryl alcohol in near-critical isopropanol over Cu/MgO-Al2O3 catalyst, Mol. Catal. 445 (2018) 94–101. https://doi.org/10.1016/j.mcat.2017.11.011.

[9] P. Jia, X. Lan, X. Li, T. Wang, Highly Active and Selective NiFe/SiO2Bimetallic Catalyst with Optimized Solvent Effect for the Liquid-Phase Hydrogenation of Furfural to Furfuryl Alcohol, ACS Sustain. Chem. Eng. 6 (2018) 13287–13295. https://doi.org/10.1021/acssuschemeng.8b02876.

[10] Y. Wang, P. Prinsen, K.S. Triantafyllidis, S.A. Karakoulia, P.N. Trikalitis, A. Yepez, C. Len, R. Luque, Comparative Study of Supported Monometallic Catalysts in the Liquid-Phase Hydrogenation of Furfural: Batch Versus Continuous Flow, ACS Sustain. Chem. Eng. 6 (2018) 9831–9844. https://doi.org/10.1021/acssuschemeng.8b00984.

[11] Y. Wang, P. Prinsen, K.S. Triantafyllidis, S.A. Karakoulia, A. Yepez, C. Len, R. Luque, Batch versus Continuous Flow Performance of Supported Mono- and Bimetallic Nickel Catalysts for Catalytic Transfer Hydrogenation of Furfural in Isopropanol, ChemCatChem. 10 (2018) 3459–3468. https://doi.org/10.1002/cctc.201800530.

[12] J. He, S. Yang, A. Riisager, Magnetic nickel ferrite nanoparticles as highly durable catalysts for catalytic transfer hydrogenation of bio-based aldehydes, Catal. Sci. Technol. 8 (2018) 790–797. https://doi.org/10.1039/C7CY02197F.

[13] F. Wang, Z. Zhang, Catalytic Transfer Hydrogenation of Furfural into Furfuryl Alcohol over Magnetic γ-Fe_2O_3 @HAP Catalyst, ACS Sustain. Chem. Eng. 5 (2017) 942–947. https://doi.org/10.1021/acssuschemeng.6b02272.

[14] T. Su, R. Peng, Z.D. Hood, M. Naguib, I.N. Ivanov, J.K. Keum, Z. Qin, Z. Guo, Z. Wu, One-Step Synthesis of Nb2O5/C/Nb2C (MXene) Composites and Their Use as Photocatalysts for Hydrogen Evolution, ChemSusChem. 11 (2018) 688–699. https://doi.org/10.1002/cssc.201702317.

Table S.2 XPS peak fitting results for Nb_4C_3Tx before testing derived from Figure 6 a and c.

Region	BE (eV)	FWHM (eV)	Fraction	Assigned to	Ref. for assignation
Nb $3d_{5/2}$ ($3d_{3/2}$)	203.2 (205.7)	1.2 (0.8)	0.21	($Nb^{\ddagger}$)	J. Halim, et al. Appl. Surf. Sci. 2016, 362, 406-417.
	203.5 (206.3)	0.7 (0.8)	0.18	Nb*	
	203.8 (20.8)	0.6 (0.7)	0.18	Nb^{+}	
	204.2 (207.3)	0.4 (0.8)	0.14	Nb^{2+}	
	204.4 (207.7)	0.4 (0.7)	0.08	Nb^{3+}	
	204.7 (208.3)	0.4 (0.8)	0.09	Nb^{4+}	
	205.0 (208.8)	0.5 (0.8)	0.06	Nb_2O_5	
	205.3 (209.3)	0.5 (0.5)	0.05	C-Nb-F	

O 1s	530.2	1.4	0.21	Nb_2O_5	
	530.8	1.3	0.21	C-Nb-O_x	
	531.4	1.1	0.16	C-Nb-$(OH)_x$	
	532.1	0.7	0.06	AlO_x	
	533.1	1.6	0.26	H_2O	
	534	2.0	0.1	$Al(OF)_x$	

Table S.3 XPS peak fitting results for Nb_4C_3Tx after testing derived from Figure 6 b and d.

Region	**BE (eV)**	**FWHM (eV)**	**Fraction**	**Assigned to**	**Ref.**
Nb $3d_{5/2}$ ($3d_{3/2}$)	203.2 (205.7)	1.3(1.0)	0.27	($Nb^{‡}$)	J. Halim, et al. Appl. Surf. Sci. 2016, 362, 406-417.
	203.4 (206.2)	0.7(0.8)	0.17	Nb*	
	203.8 (206.7)	0.6(0.7)	0.18	Nb^{+}	
	204.0 (207.1)	0.4 (0.6)	0.09	Nb^{2+}	
	204.2 (207.5)	0.4 (0.7)	0.08	Nb^{3+}	
	204.4 (208.0)	0.4 (0.8)	0.08	Nb^{4+}	
	204.7 (208.5)	0.6 (0.6)	0.06	Nb_2O_5	
	205.0 (208.9)	0.7 (0.5)	0.06	C-Nb-F	
O1s	530.3	1.4	0.18	Nb_2O_5	
	530.9	1.1	0.19	C-Nb-O_x	
	531.5	1.1	0.18	C-Nb-$(OH)_x$	
	532.3	1.1	0.15	AlO_x	
	533.3	1.1	0.17	H_2O	
	534.1	1.3	0.14	$Al(OF)_x$	

Table S.4 XPS peak fitting results for Nb_2CT_x after testing derived from Ref.[14]

Region	**BE (eV)**	**Assigned to**	**Ref.**
Nb $3d_{5/2}$	202.9 (205.9)	($Nb^{‡}$)	J. Halim, et al.
	203.4 (206.2)	Nb*	
($3d_{3/2}$)	203.8 (206.6)	Nb^{+} , Nb^{2+}, Nb^{4+}	Appl. Surf. Sci.
	204.4 (207.3)	NbO	2016, 362, 406-417.
	205.5 (208.4)	Nb^{3+} - O	
	206.8 (209.5)	Nb^{4+} - O	
	207.7 (210.4)	Nb_2O_5	
O1s	529.9	Nb_2O_5	
	530.9	Nb – C – O_x	
	531.8	C-Nb-$(OH)_x$	
	533.0	H_2O_{ads}	

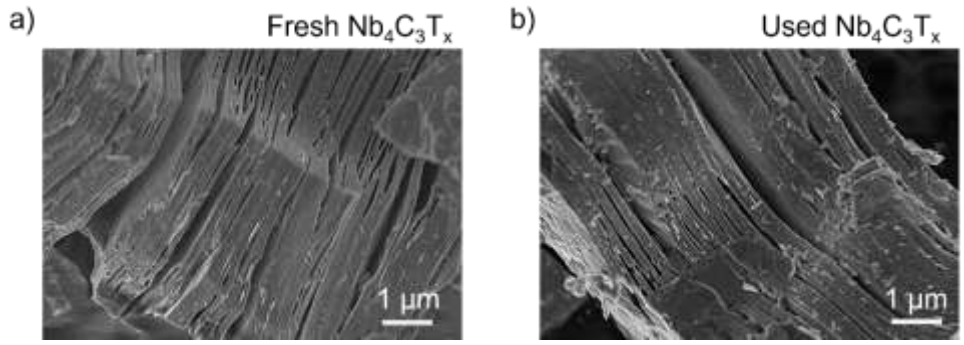

Fig. S.1 SEM characterization of Nb_4C_3 MXenes before and after testing

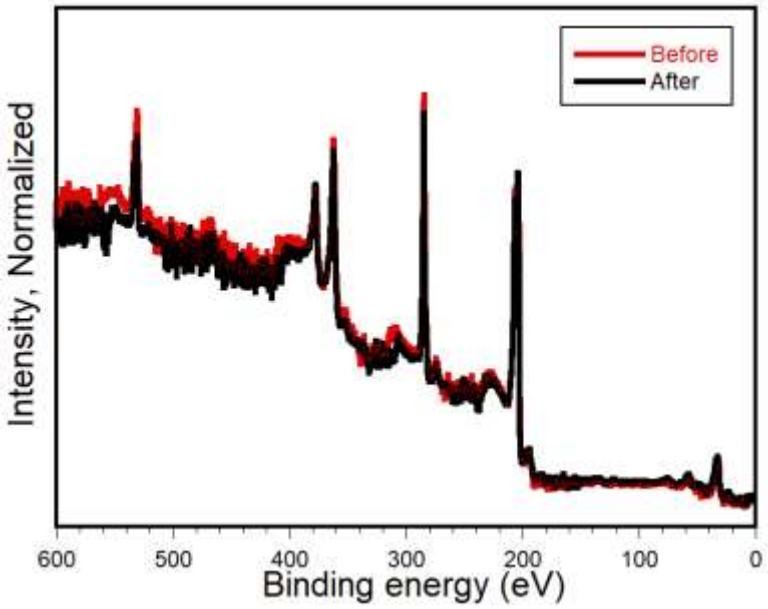

Figure S.2 XPS survey of Nb_4C_3 MXenes before and after testing.